energies

MDPI

Article

# A Comprehensive Control Strategy for a Push–Pull Microinverter Connected to the Grid †

**Manuel Díaz [1], Javier Muñoz [2,*], Marco Rivera [2,3] and Jaime Rohten [4]**

1 Engineering Sciences Master's Program, Faculty of Engineering, University of Talca, Curicó 3340000, Chile
2 Faculty of Engineering, University of Talca, Curicó 3340000, Chile
3 Faculty of Engineering, University of Nottingham, 15 Triumph Rd, Lenton, Nottingham NG7 2GT, UK
4 Department of Electrical and Electronic Engineering, University of Bío-Bío, Concepción 4051381, Chile
* Correspondence: jamunoz@utalca.cl

† This paper is an extended version of our paper published in 2022, International Symposium on Power Electronics, Electrical Drives, Automation and Motion (SPEEDAM), Sorrento, Italy, 22–24 June 2022; pp. 883–888.

**Abstract:** The effects of partial shading or dust accumulation on the panels of photovoltaic systems connected to the grid can generate a considerable reduction in energy performance, being necessary to provide the appropriate voltage to the grid regardless of the irradiance level. This paper addresses this problem and presents a comprehensive control strategy and its implementation for a grid-connected microinverter composed of a push–pull converter followed by an H-bridge inverter. In the push–pull converter, a hybrid MPPT algorithm and a PI control enable work in the MPP of the PV panel. In the H-bridge inverter, a cascade control consisting of a PI control and a predictive control allows the connection to the grid. A proof-of-concept prototype is implemented in order to validate the proposal. Experimental tests were performed by connecting the microinverter to a PV panel and a programmable photovoltaic panel emulator to check the MPPT performance. Furthermore, partial shading conditions were simulated on the *dc* source to check if the global maximum power point is reached. Experimental results demonstrate the feasibility of the topology and the control approach, obtaining MPPT performance in the topology above 99% at different power and voltage levels on the MPPT, even in the presence of partial shading conditions.

**Keywords:** microinverter; MPPT algorithm; push–pull converter; renewable energy



**Citation:** Díaz, M.; Muñoz, J.; Rivera, M.; Rohten, J. A Comprehensive Control Strategy for a Push–Pull Microinverter Connected to the Grid. *Energies* **2023**, *16*, 3196. https://doi.org/10.3390/en16073196

Academic Editors: José Matas, Md Rasheduzzaman and David Macii

Received: 7 November 2022
Revised: 17 March 2023
Accepted: 20 March 2023
Published: 1 April 2023



## 1. Introduction

Nowadays, renewable energy systems are critical to achieving sustainable development goals to accelerate social progress in the world. Due to the development that has been achieved in photovoltaic (PV) panel manufacturing and its continuous cost reduction as well as the advances in power electronics, PV distributed power generation has become highly competitive among other renewable energy systems [1–3]. A power converter is needed to transfer the energy obtained from the PV panel to the grid or to feed a local load, e.g., for residential use. Grid-connected converters in PV systems can be classified into central inverters, string inverters, and modular AC converters, also known as microinverters [4]. In PV applications where central inverters, string inverters, or multi-string inverters are used, the overall system efficiency can be considerably decreased if a module is defective or subject to partial or total shading condition; this is because the inverter cannot reach the maximum power point (MPP) of each PV module, due to the series configuration in which they are connected [5,6]. Shading effects can also be generated by dust or snow accumulation on PV panels [7]. Microinverters allow obtaining an individual MPP of each PV panel which contributes to increase the system performance, extracting the maximum power from each module individually [8,9]. Several algorithm schemes have been proposed in microinverters to work in the MPP of the photovoltaic panel [10–13]. Various MPPT control algorithms are proposed in the existing literature to deal with PV systems operating under partial shading conditions. In [14], the chaos search theory is first applied to the MPPT technology of PV systems, improving search efficiency and solving the multiple MPP problem under partial shading conditions. In [15], the simulated annealing method is proposed. The performance is assessed by considering the time taken to converge and the number of sample cases the technique finds the GMPP. Simulation results indicate the improved performance of the simulated annealing-based algorithm. In [16], the ABC algorithm for the MPPT of a PV system using a DC–DC converter is proposed. The ABC MPPT algorithm uses data values from the PV module, identifies the P-V characteristic, and selects the optimal voltage. This method archives superior performance compared with conventional methods. In [17], a hybrid algorithm used in a push–pull-based pseudo DC-link PV microinverter was evaluated, reaching a simulation performance close to 99%. Another converter can be used using the same MPPT. For example, [12], the Flyback converter is employed. There is no restriction on the converter to be used because a short circuit is never generated in the panel, or the panel is never disconnected from the converter (some algorithms need to perform these actions to obtain the MPP, for example, the fractional open circuit voltage (FOCV) and fractional short circuit current (FSCC) method) [18,19]. The disadvantage of the proposed scheme is that it will continuously oscillate even when the GMPP is reached (smaller oscillations will be generated). In [20], an active way to find the global MPP is presented, by searching the local MPPs with a measuring cell algorithm and then improving the location of the GMPP with an enhanced perturb and observe method to be as close as they can to the MPP.

In the microinverter, the transformerless topologies generally demonstrate advantages in terms of high efficiency, low cost, simplicity, and compactness [21,22]. However, due to the lack of galvanic isolation, such inverters cannot support dual grounding of both DC and AC, and also may exhibit ground leakage current. A transformer in a microinverter is the immediate solution to eliminate leakage current flowing from the PV panel. In addition, physical isolation between the PV module and the grid in some of the microinverter topologies eliminates all the problems of the dual grounding requirement [23–25].

Different topologies of push–pull microinverters have been proposed [26–29]. These topologies vary in the conformation of the push–pull converter or the forms that the DC-link is implemented. In [26], a push–pull-based pseudo DC-link PV microinverter is presented, characterized by replacing the electrolytic capacitor in the DC-link with an inductor to control the current. In [27], a modified integrated buck and push–pull converter is proposed, which can reduce the voltage level on the primary side of the transformer. The converter is used to supply a local load and not to connect to the grid. In [28], a single-stage microinverter topology based on a push–pull converter integrated with a quasi-Z source network and coupled with a voltage unfolder is presented, which does not use a DC-link in its structure. In [29], a push–pull microinverter based on a submodular structure is presented, which connects three push–pull converters to an H-bridge inverter to generate alternating current at the microinverter AC side. In [30], a current-fed push–pull quasi-resonant converter is proposed. However, the converter is not used with photovoltaic panels and does not have a grid connection. Different controls have been proposed depending on how the push–pull microinverter is constituted. In [26], a P&O algorithm is used with a PI and a PR control to control the current injected into the grid. In [29], PI control for each push–pull converter that makes up the topology structure and predictive control for the H-bridge inverter are presented, but there are no results of the grid connection.

The main contribution of this work lies in the development and implementation of a comprehensive control strategy for a push–pull microinverter prototype, which allows working on the MPP of the photovoltaic panel and injecting the obtained power into the grid. The proposed control guarantees a stable voltage on the DC-link regardless of the irradiance in the PV panel. Moreover, the control used is independent of the transformer ratio, which makes it versatile for a large number of transformers.

## 2. Overall System Model

The topology proposed in this work is conformed by a PV panel that is connected to the push–pull converter. It requires a high frequency transformer with a central connection on both the primary and secondary sides. The DC link voltage $(v_{dc})$ generated at the transformer's secondary is supported by capacitor $C$. An H-bridge inverter is attached for interconnection to the grid, which allows transforms the DC power into AC power through an appropriate control. The proposed topology is shown in Figure 1a.

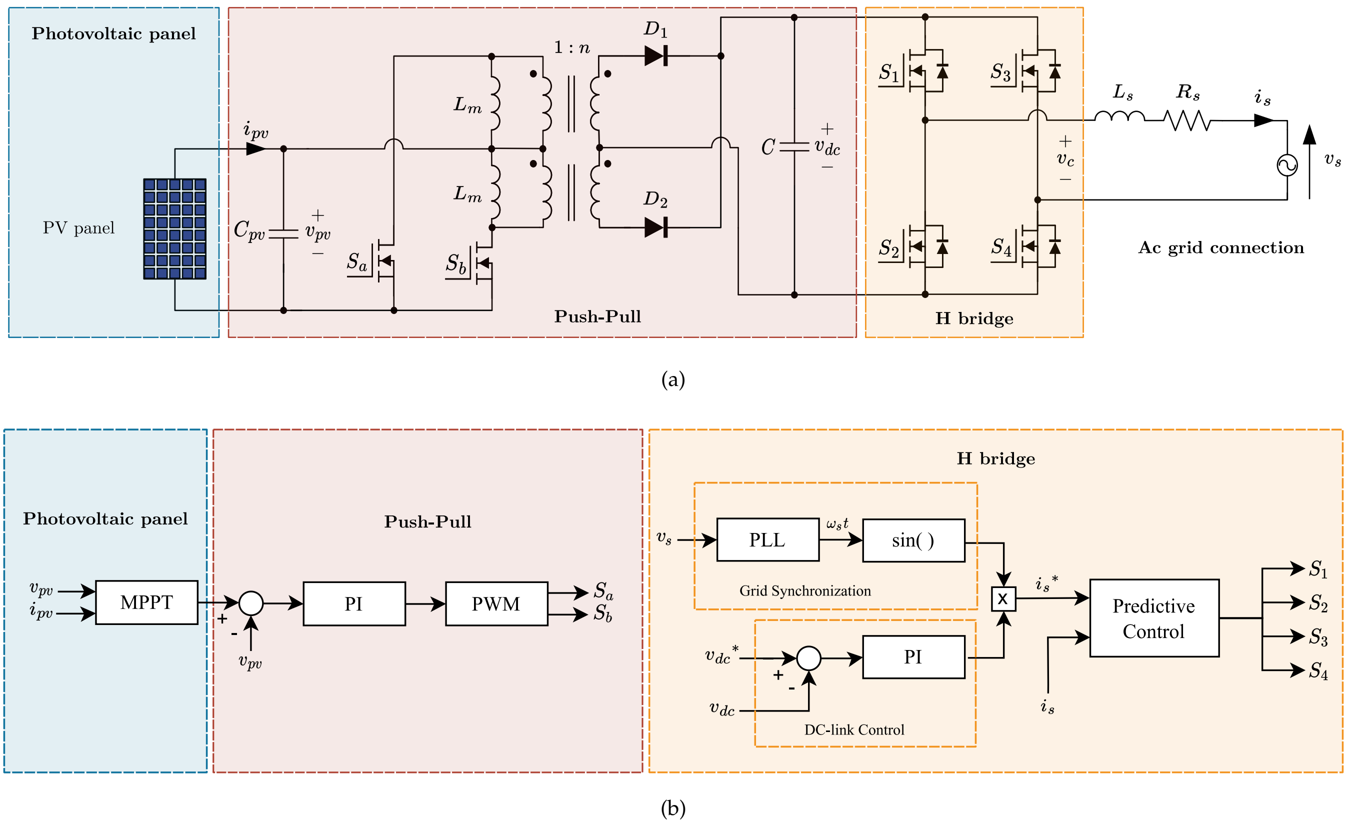


**Figure 1.** (**a**) Push–pull microinverter, (**b**) control applied in the topology.

The operation of the transformer in the push–pull converter is as follows, when the semiconductor $S_a$ is closed, current flows through the upper half of the transformer primary winding. The magnetic field of the transformer expands and binds to the secondary winding, inducing a voltage in the secondary winding, $D_2$ is direct biased conducting and charging the capacitor, while $D_1$ is reverse biased so it does not conduct. By contrast, when the semiconductor $S_b$ is closed, current flows through the lower half of the primary winding of the transformer, $D_1$ conducts and charges the capacitor, while $D_2$ is reverse biased. Despite the transformer reduced the total system efficiency, it has some other advantages, such as the isolation between the PV systems and the H-Bridge system, making it possible to extend this topology to a multilevel one, stacking the H-bridge avoiding short circuits.

The transformer transformation radio is arbitrary but fixed. Therefore, in most circuit implementations, the duty cycle of the semiconductors $S_a$ and $S_b$ can be varied to modify the range of voltage ratios through the following equation,

$$v_{dc} = v_{pv} \cdot \frac{N_2}{N_1} \cdot f_s \cdot (t_1 + t_2) \tag{1}$$

where,

- $v_{dc}$ = DC-link voltage.

- $v_{pv}$ = PV panel voltage.
- $N_2$ = number of secondary turns.
- $N_1$ = number of primary turns.
- $f_s$ = switching frequency (Hz).
- $t_2$ = time period of $S_a$ conduction (seconds).
- $t_1$ = time period of $S_b$ conduction (seconds).

In this work, the push–pull has the function of controlling the voltage in the $C_{pv}$ capacitor in order to work on the MPP of the PV panel by switching of semiconductors $S_a$ and $S_b$. The H bridge inverter allows to convert the DC power obtained from the PV panel through the push–pull converter into AC power to be fed into the grid.

## 3. Power Converters Controllers

### 3.1. Push–Pull Control

In Figure 1b, it is possible to see the control scheme implemented in the push–pull microinverter. The PI control has the purpose of controlling the voltage in the PV panel to reach the MPP, which is performed by varying the gating patterns of the semiconductors $S_a$ and $S_b$, having the same duty cycle but phase shifted in 180°, and the maximum duty cycle is 0.5. The control receives as reference the difference between the output of the MPPT algorithm and the voltage in the PV panel ($v_{pv}$), and the output of the PI controller generates the modulating signal that feeds the PWM generator. It is important to highlight that the employed algorithm is always oscillating around the MPP, even if it has already found the MPP, which is the main reason that this algorithm never will have a unitary efficiency.

### 3.2. H-Bridge Control

The control of the H-bridge converter has three main functions, to synchronize the converter to the power grid, control the DC-link voltage, and generate the AC at the H-Bridge inverter. The control is composed of a PLL for the synchronization with the grid, which receives the grid voltage $(v_s)$ and generates a sinusoidal signal with unit amplitude. A cascade control consisting of a PI control and a predictive control is used for controlling the DC-link voltage. The cascade control receives the difference between the voltage reference $(v_{dc}{}^*)$ and the voltage in the DC-link $(v_{dc})$, and gives the amplitude to the reference current of the slave predictive control $(i_s{}^*)$. The predictive control is incorporated to manage the H-Bridge AC current, which is performed by switching the semiconductors $S_1$, $S_2$, $S_3$, and $S_4$. The AC inverter Kirchhoff voltage Law can be written as follows,

$$v_c = L_s \cdot \frac{di_s}{dt} + R_s \cdot i_s + v_s \tag{2}$$

The value of $v_c$ is the H-Bridge power converter injected voltage, which depends on the switching state of the semiconductors $S_1$, $S_2$, $S_3$, and $S_4$. Table 1 shows the possible values.

**Table 1.** Possible switching states.

| State | $S_1$ | $S_2$ | $S_3$ | $S_4$ | $v_c$ |
|---|---|---|---|---|---|
| 1 | 0 | 1 | 0 | 1 | 0 |
| 2 | 0 | 1 | 1 | 0 | $-v_{dc}$ |
| 3 | 1 | 0 | 0 | 1 | $v_{dc}$ |
| 4 | 1 | 0 | 1 | 0 | 0 |

The approximate first order discrete model in terms of AC H-bridge is given by,

$$\frac{di_s}{dt} = \frac{i_{s[k+1]} - i_{s[k]}}{T_s} \tag{3}$$

Replacing (3) in (2) and simplifying we obtain the expression (4),

$$i_{s[k+1]} = \frac{v_{c[k]} \cdot T_s}{L_s} + (1 - \frac{T_s \cdot R_s}{L_s}) i_{s[k]} - \frac{v_{s[k]} \cdot T_s}{L_s} \tag{4}$$

where,

- $i_{s[k+1]}$ = predicted AC H-Bridge current a next step.
- $i_{s[k]}$ = AC H-Bridge current.
- $T_s$ = sampling time.
- $L_s$ = AC H-Bridge inductance.
- $R_s$ = AC H-Bridge resistor.
- $v_{c[k]}$ = AC H-Bridge voltage.
- $v_{s[k]}$ = grid voltage.

The cost function established in the predictive control, allows to evaluate which switching state generates a smaller difference between (4) and the reference current provided to the control $(i_s{}^*)$. In Equation (5), it is possible see the cost function considered in this work.

$$G = |i_s{}^* - i_{s[k+1]}| \tag{5}$$

## 4. MPPT Algorithm

The hybrid MPPT algorithm used in this work was presented in [12]. It is composed of the conventional algorithms perturb and observe (P&O) and incremental conductance (IC). The algorithm is characterized by a variable step size, converging faster to MPP compared to conventional methods. This is because, after changing the voltage reference, it evaluates the slope P-V curve tested. If the slope is higher than the slope previously tested, it implies that it is far from the MPP, so it establishes a larger step size to reach the desired point faster. In the opposite case, if it is near the MPP, it will set a smaller step size to obtain the MPP point. Once the MPP is reached, small perturbations continue to be made on the reference voltage to leave this point in case an local MPP is achieved and not the global MPP. However, these variations do not cause a significant decrease in the power obtained from the PV panel [17]. Figure 2 shows the algorithm used in this work.

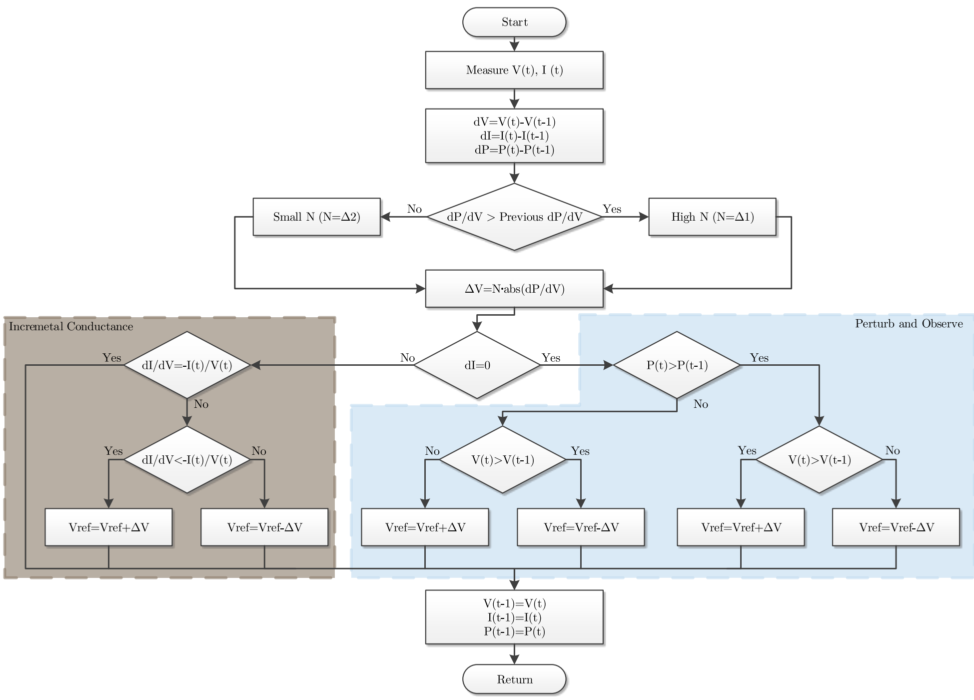


**Figure 2.** Hybrid MPPT applied to push–pull microinverter.

Table 2 shows a comparison between the MPPT algorithms that work under partial shade conditions. As can be seen, all the algorithms oscillate around the MPP, and therefore, their efficiency is always lesser than the unitary, but the one chosen in this work has a medium complexity which makes it better for microinverter applications because it can be employed a cheaper digital board.

**Table 2.** MPPT algorithm comparison.

| Algorithm MPPT | Efficiency | Tracking Speed | Presents Optimization Function | Perturbations in the Operating Point (Voltage) | Implementation Complexity |
|---|---|---|---|---|---|
| Chaotic Search | High | High | Yes | Yes | High |
| ABC | High | High | No | Yes | Medium |
| Simulated Annealing | High | High | Yes | Yes | High |
| Hybrid MPPT (this work) | High | High | No | Yes | Medium |

## 5. Results

Experimental results to demonstrate the feasibility of the control scheme in the push–pull microinverter are obtained using the following equipment:

- Chroma 62020H-150S programmable power supply.
- Photovoltaic panel model type A-255 GS (Atersa). The electrical ratings are:
  - Maximum Power $(P_{mpp})$ : 255 Wp.
  - Open Circuit Voltage $(V_{oc})$ : 37.83 V.
  - Short Circuit Current $(I_{sc})$ : 8.97 A.
  - Maximum Power Voltage $(V_{mpp})$ : 30.29 V.
  - Maximum Power Current $(I_{mpp})$ : 8.42 A.
- Optical fiber receptor to command power switches, allowing fast communication and EMI/RFI immunity, among others.
- FPGA Basys3 (for generated the dead times in the power switches).
- TMS320F28335 Digital Signal Controllers.

Table 3 shows the description of the main components used in the push–pull converter and the H bridge inverter.

**Table 3.** Components used in this work.

| Component | Description |
|---|---|
| Power switches $S_a$, $S_b$, $S_1$, $S_2$, $S_3$ and $S_4$ | CREE C2M0080120 |
| Rectifier diode $D_1$, $D_2$ | RURG80100 |
| High frequency transformer | ETD-49 |
| Electrolytic capacitor $C$ | 10 mF 50 V |
| Electrolytic capacitor $C_{pv}$ | 100 uF 450 V |

Figure 3 shows the real push–pull microinverter used in this work.
The numbering corresponds to:

- 1: Power supply (for instrumentation).
- 2: AC current sensors.
- 3: DC voltage sensors.
- 4: Push–pull converter.
- 5: Trigger card.
- 6: FPGA Basys3.
- 7: DSP TMS320F28335.
- 8: AC voltage sensor.
- 9: H bridge inverter.

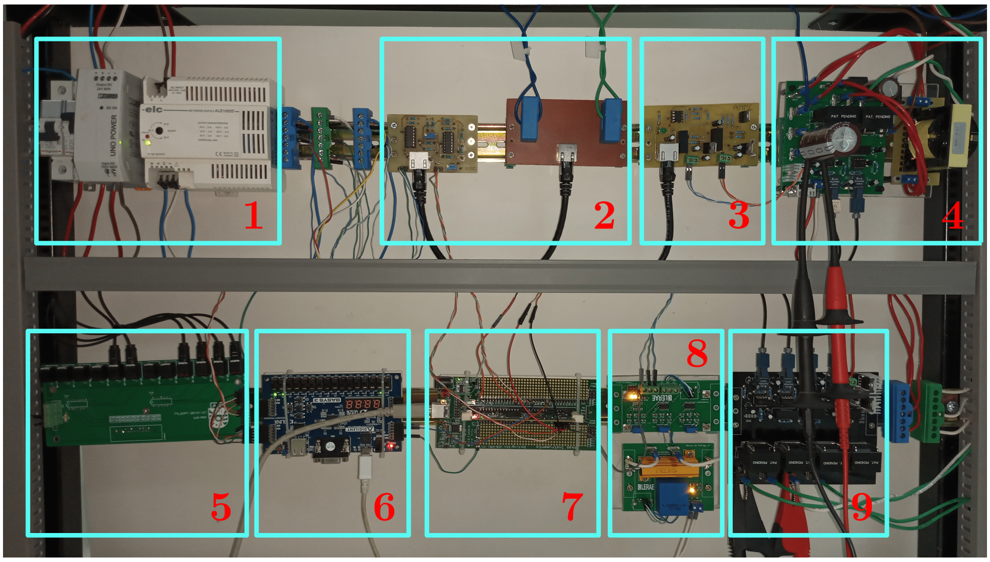


**Figure 3.** Implementation of the push–pull microinverter.

To corroborate the current control loop, the programmable source was set to be a DC source, keeping the DC voltage constant and independent of the drained power. Thus, Figure 4 shows the response of the microinverter current control loop, considering a transformer with ratio $n = 1$ is used. In the picture, it is possible to see that the capacitor voltage $V_{pv}$ is similar to the $V_{mpp}$ panel, which is 30.29 V, and the proposed control works when a change in the reference current is generated.

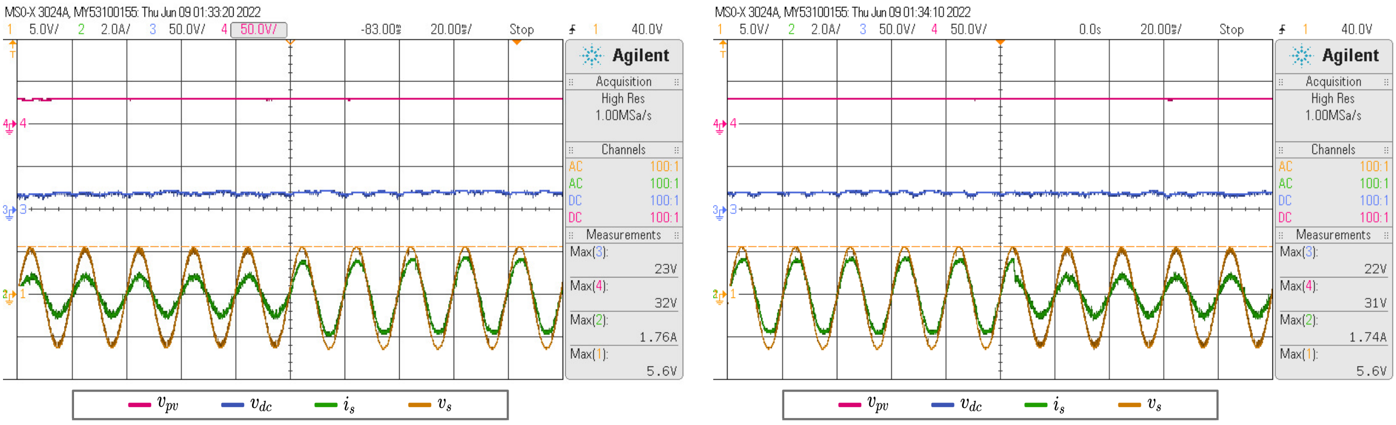


(a) (b)

**Figure 4.** (**a**) Control response with an increase in reference current, (**b**) control response with a decrease in reference current.

Figure 5 shows the commutations in the semiconductors of the push–pull converter and H bridge inverter. In the picture, it is possible to see that the semiconductors $S_a$ and $S_b$ have the same duty cycle but phase shifted in 180°.

Figure 6 shows two simulated curves of different voltage and power loaded into the Chroma programmable power supply. Both loaded curves have different power and Vmpp points. Once loaded, these voltage and power values are provided directly by the Chroma programmable power supply to the microinverter. In these images, we can see that in both cases, the voltage and current measured on the panel (Vmea and Imea) are similar to the Vmpp and Impp of the loaded curve, obtaining an MPPT efficiency of 99.33% in the 150 W PV panel and 99.83% when the PV panel is 60 W. Thus, as the MPPT algorithm is always oscillating around the MPP, the efficiency would return a number lesser than the unitary.

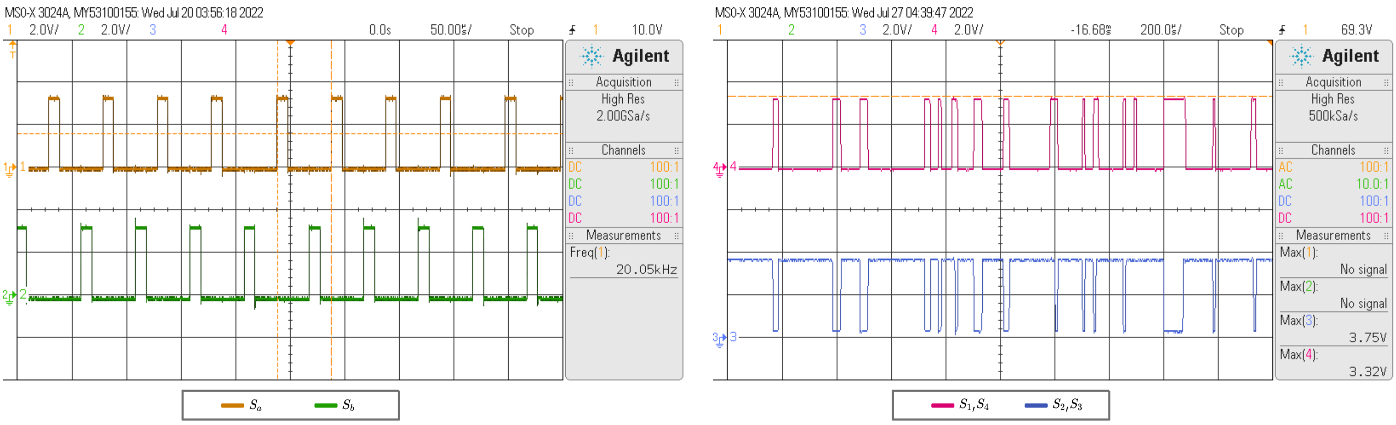


(a) (b)

**Figure 5.** (**a**) Commutations in the semiconductors on the push–pull converter, (**b**) commutations in the semiconductors on the H bridge inverter.

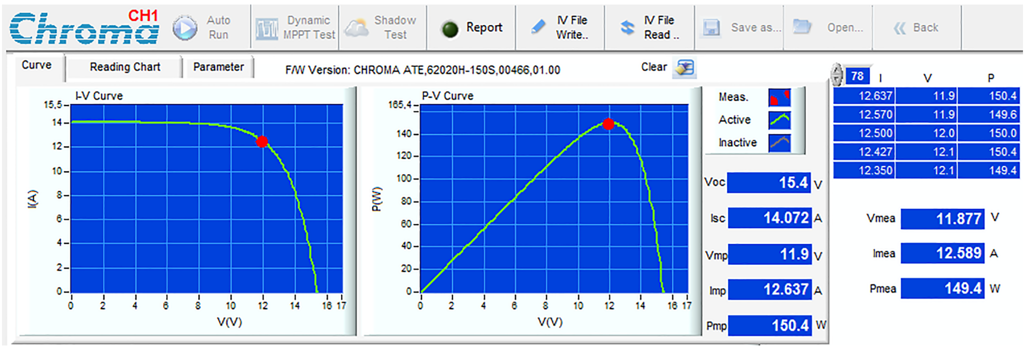


(a)

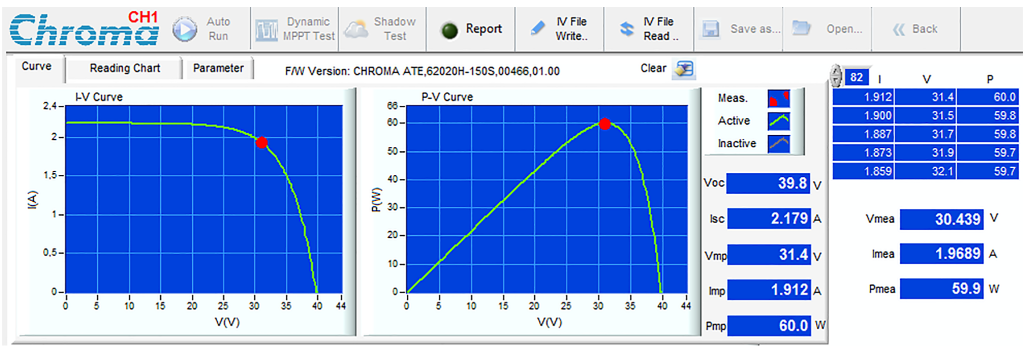


(b)

**Figure 6.** (**a**) MPPT performance in the emulation of a 150.4 W PV panel, (**b**) MPPT performance in the emulation of a 60 W PV panel.

Figure 7 shows the response of the microinverter when an elevator transformer is used in the topology. In Figure 7a, we can see that the voltage on the capacitor $(v_{dc})$ is greater than the voltage on the PV panel $v_{pv}$, which shows the boost capabilities of the push–pull converter. It can also be seen that the voltage at the PV panel is similar to the $V_{mpp}$ that the Chroma source shows Figure 6a. Furthermore, it is possible to see that the current injected into the grid $i_s$ is in phase with the grid voltage $v_s$. From Figure 7b, we can see the effects of a change in the reference amplitude of the current injected into the grid, which does not affect the control in the microinverter.

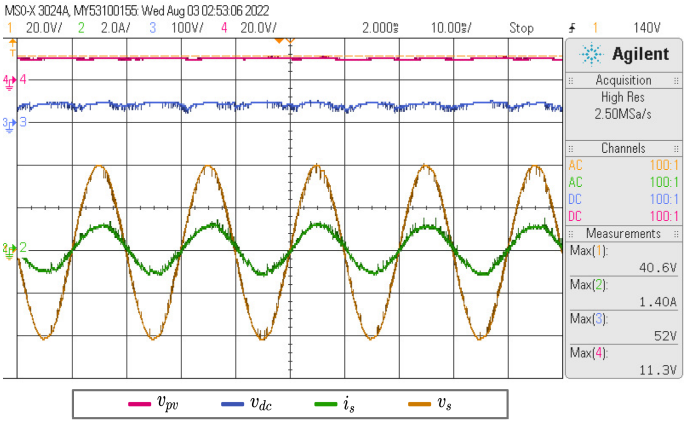


(a) (b)

**Figure 7.** (**a**) Waveforms of voltage and current in the microinverter, (**b**) waveforms of voltage and current in the microinverter with change of the referent current.

Partial shading effects was simulated to check the hybrid MPPT used in this work. Figure 8 shows the simulated voltage and power curves loaded in the Chroma programmable source. In the picture, it is possible to see that the hybrid MPPT allows finding in the PV panel the global MPP and no the local MPP. Further, it is possible to see that the voltage and current measured in the panel ($V_{mea}$ and $I_{mea}$) are similar to the $V_{mpp}$ and $I_{mpp}$, obtained a 99.75% performance of the MPPT.

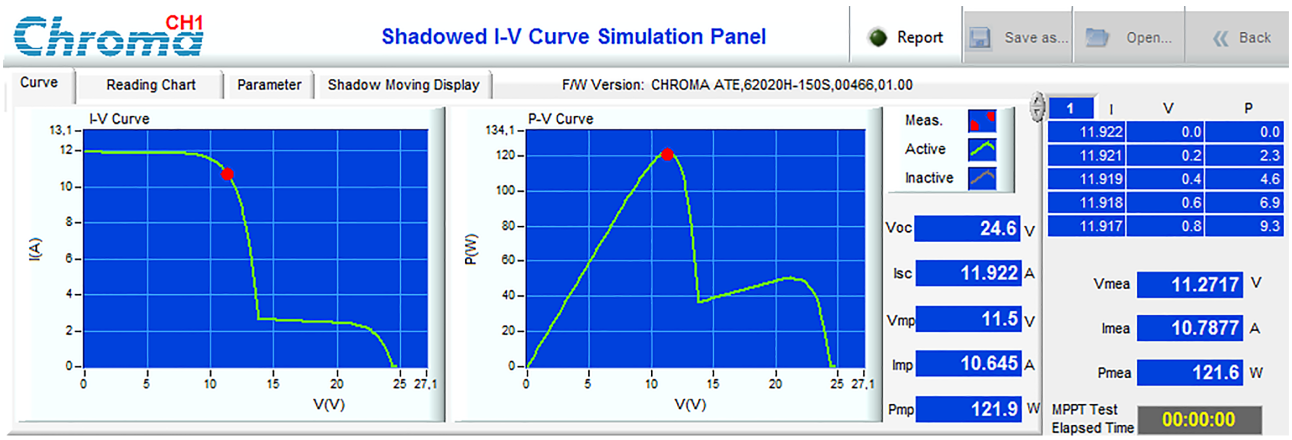


**Figure 8.** Simulated partial shading.

Figure 9 shows the grid's voltage and current when using the partial shading effect of Figure 8.

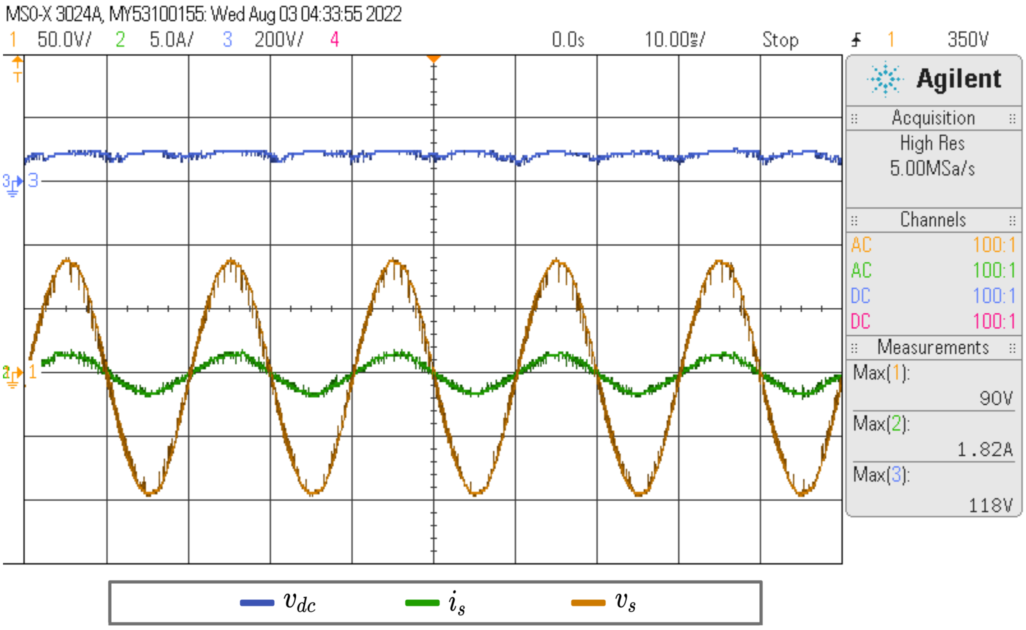


**Figure 9.** Waveforms of voltage and current in the grid.

## 6. Discussion

Efficiency and reliability are very relevant aspects in microinverters, but in addition, grid-connected PV systems must take into account safety considerations, in particular, grounding and ground leakage currents, which are generated from the potential difference that appears between the PV module and the neutral of the grid depending on the switching of the inverter. There are two possibilities for the generation of the leakage current. If the PV module terminals are grounded due to potential difference, there will be a high leakage current. The other option is that the PV module terminals are not connected to ground, which generates a high frequency voltage across the capacitors, which in turn generates a high leakage current. One technique to suppress leakage current is that during the no-load time interval, the PV module and the grid should be separated, dividing the input voltage by two DC link capacitors connected to the grid neutral; thus, it will block the common mode voltage, and directly connecting the negative terminal of the PV module and the neutral of the network. In [31], an investigation of single-stage transformerless buck-boost microinverters is carried out. The authors mention the high efficiency of the microinverter, as well as the problems generated by the circulating current in the topology and the precautions to be taken, establishing that the best solution is to interconnect the negative photovoltaic terminal with the grid neutral and double grounding. In [32], the effects and consequences of the circulating current are analyzed in the transformerless boost microinverter. In [33,34], the consequences of leakage current and leakage inductance in the Sepic-Ćuk microinverter are analyzed. The advantage of using the pull–pull topology is that it eliminates the problems caused by leakage current flowing from the PV panel to ground through parasitic capacitors in non-isolated single-stage microinverters, due to the fact that the topology of the microinverter push–pull uses a transformer in its architecture. Additionally, the physical isolation between the PV module and the grid in some of the microinverter topologies eliminates all challenges of the double grounding requirement. The push–pull microinverter features low ripple voltage on the DC solar side and reduces the stress under which semiconductors switch compared to single-stage microinverters and eliminates the inconveniences generated by the circulating current in the transformer as it uses a center tap transformer on both the primary and secondary side. Likewise, the leakage inductance presents in isolated topologies with transformers without a central tap, such as the one established by the Flyback microinverter, is eliminated producing the cancellation of the harmful effects of the leakage inductance.

In microinverters, one of the main objectives is to work under partial shading conditions to extract the maximum PV power to inject into the grid. In a photovoltaic panel, various points of maximum power can be formed, where there will always be a global GMPP point, and the others will be local LMPP points. The challenge for the microinverter's to distinguish if it is operating at the GMPP. Conventional algorithms of MPPT cannot differentiate whether it is a local or global maximum. The hybrid algorithm used in this work differentiates these points, contributing to better energy harvesting from the PV panels.

In the presented push–pull topology and with the applied control, transformers with different ratios can be used. This does not affect the current injected into the grid or the control to find the MPP. Only the voltage in the DC-link change due to the use of different transformers, which can be successfully overcome with the proposed control technique.

In the obtained results, we can observe that the DC-link voltage presents a harmonic component of twice the grid frequency, which is a characteristic of the double-stage single-phase microinverters [35–37]. Furthermore, different amplitude changes in the current injected into the grid were considered, which did not affect the behavior of the DC-link.

## 7. Conclusions

In this work, the hybrid MPPT algorithm used allows obtaining the GMPP in the photovoltaic panel, which conventional algorithms cannot ensure. Furthermore, a PI control, together with the MPPT used, allows controlling the push–pull converter, while the predictive control used in the H-bridge inverter controls the DC-link voltage and the current injected into the grid.

Using a center tap transformer on both the primary and secondary sides reduces the efficiency of the microinverter compared to non-isolated single stage topologies. Its incorporation eliminates the inconveniences generated by the circulating current in the transformer. In addition, it generates isolation between the converter and the inverter, allowing a more secure connection to the grid.

The experimental implementation validates the proposed control strategy that allows the independent operation of the push–pull converter with the H-bridge inverter, thus establishing a decoupled control, which is the main advantage of the proposal since this does not restrict the transformer transformation ratio used in the topology. Another significant advantage is that a different control could also be used on the H-bridge inverter, for example, a resonant proportional control, which would not affect the control set on the push–pull converter.

The proposed control strategy allows to operate at the global maximum power point and inject power to the grid decoupled from the PV panel variations, obtaining an MPPT efficiency higher than 99%, even if it is subject to partial shading conditions. The hybrid MPPT algorithm was also used with different operating voltages and power levels in the MPPT, obtaining satisfactory performance in all cases.

**Author Contributions:** Conceptualization, M.D., J.M., M.R. and J.R.; Methodology, M.D., M.R. and J.R.; Software, J.M.; Validation, M.D.; Formal analysis, J.R.; Investigation, M.D., J.M. and M.R.; Resources, J.M.; Writing—original draft, M.D.; Writing—review & editing, J.M., M.R. and J.R.; Supervision, J.M.; Project administration, J.M.; Funding acquisition, J.M. All authors have read and agreed to the published version of the manuscript.

**Funding:** This paper is partially supported by the Chilean government through the project ANID/FONDECYT/1191028, Fondap Solar Energy Research Center N°15110019 project, CLIMAT AMSUD 210001 project and the Lakehead University student exchange program under Global Affairs Canada—Emerging Leaders of the Americas Scholarship program 2021–2022.

**Data Availability Statement:** Not applicable.

**Conflicts of Interest:** The authors declare no conflict of interest.

## Abbreviations

The following abbreviations are used in this manuscript:

| | |
|---|---|
| MPPT | Maximum Power Point Tracking |
| MPP | Maximum Power Point |
| GMPP | Global Maximum Power Point |
| LMPP | Local Maximum Power Point |
| P&O | Perturb and Observe |
| IC | Incremental Conductance |

## References


1. Shafiullah, M.; Ahmed, S.D.; Al-Sulaiman, F.A. Grid Integration Challenges and Solution Strategies for Solar PV Systems: A Review. *IEEE Access* **2022**, *10*, 52233–52257. [CrossRef]
2. Tang, Z.; Yang, Y.; Blaabjerg, F. Power electronics: The enabling technology for renewable energy integration. *CSEE J. Power Energy Syst.* **2022**, *8*, 39–52.
3. Sutikno, T.; Arsadiando, W.; Wangsupphaphol, A.; Yudhana, A.; Facta, M. A Review of Recent Advances on Hybrid Energy Storage System for Solar Photovoltaics Power Generation. *IEEE Access* **2022**, *10*, 42346–42364. [CrossRef]
4. Kouro, S.; Leon, J.I.; Vinnikov, D.; Franquelo, L.G. Grid-Connected Photovoltaic Systems: An Overview of Recent Research and Emerging PV Converter Technology. *IEEE Ind. Electron. Mag.* **2015**, *9*, 47–61. [CrossRef]
5. Karanayil, B.; Ceballos, S.; Pou, J. Maximum Power Point Controller for Large-Scale Photovoltaic Power Plants Using Central Inverters Under Partial Shading Conditions. *IEEE Trans. Power Electron.* **2019**, *34*, 3098–3109. [CrossRef]
6. Pendem, S.R.; Mikkili, S. Assessment of cross-coupling effects in PV string-integrated-converters with P&O MPPT algorithm under various partial shading patterns. *CSEE J. Power Energy Syst.* **2020**, *8*, 1013–1028
7. Surirey, Q.; Hernandez-Vidal, R.; Renaudineau, H.; Kouro, S.; Cabon, B. Sub-module photovoltaic microinverter with cascaded push-pull and unfolding H-bridge inverter. In Proceedings of the IEEE Southern Power Electronics Conference (SPEC), Puerto Varas, Chile, 4–7 December 2017; pp. 1–6.
8. Alluhaybi, K.; Batarseh, I.; Hu, H. Comprehensive Review and Comparison of Single-Phase Grid-Tied Photovoltaic Microinverters. *IEEE J. Emerg. Sel. Top. Power Electron.* **2020**, *8*, 1310–1329. [CrossRef]
9. Krein, P.T.; Galtieri, J.A. Active Management of Photovoltaic System Variability With Power Electronics. *IEEE J. Emerg. Sel. Top. Power Electron.* **2021**, *9*, 6507–6523. [CrossRef]
10. Sher, H.A.; Addoweesh, K.E.; Al-Haddad, K. An Efficient and Cost-Effective Hybrid MPPT Method for a Photovoltaic Flyback Microinverter. *IEEE Trans. Sustain. Energy* **2018**, *9*, 1137–1144. [CrossRef]
11. Diaz-Bernabe, J.L.; Morales-Acevedo, A. Simulation of a double-stage micro-inverter for grid-connected photovoltaic modules. In Proceedings of the International Conference on Electrical Engineering, Computing Science and Automatic Control (CCE), Mexico City, Mexico, 26–30 September 2016; pp. 1–6.
12. de Oliveira Lima, R.; Barreto, L.H.S.C.; Reis, F.E.U. Hybrid MPPT Control Applied to a Flyback Micro-Inverter Connected the Electrical Grid. In Proceedings of the IEEE International Conference on Industry Applications (INDUSCON), Sao Paulo, Brazil, 12–14 November 2018; pp. 59–64.
13. Bollipo, R.B.; Mikkili, S.; Bonthagorla, P.K. Hybrid, optimal, intelligent and classical PV MPPT techniques: A review. *CSEE J. Power Energy Syst.* **2021**, *7*, 9–33.
14. Zhou, L.; Chen, Y.; Guo, K.; Jia, F. New Approach for MPPT Control of Photovoltaic System With Mutative-Scale Dual-Carrier Chaotic Search. *IEEE Trans. Power Electron.* **2011**, *26*, 1038–1048. [CrossRef]
15. Lyden, S.; Haque, M.E. A Simulated Annealing Global Maximum Power Point Tracking Approach for PV Modules Under Partial Shading Conditions. *IEEE Trans. Power Electron.* **2016**, *31*, 4171–4181. [CrossRef]
16. González-Castaño, C.; Restrepo, C.; Kouro, S.; Rodriguez, J. MPPT Algorithm Based on Artificial Bee Colony for PV System. *IEEE Access* **2021**, *9*, 43121–43133. [CrossRef]
17. Díaz, M.; Muñoz, J.; Rivera, M.; Aliaga, R.; Rohten, J. Hybrid MPPT Control Applied to a Push-Pull based pseudo DC-link PV microinverter. In Proceedings of the European Conference on Power Electronics and Applications (EPE'21 ECCE Europe), Ghent, Belgium, 6–10 September 2021; pp. 1–7.
18. Carandell, M.; Holmes, A.S.; Toma, D.M.; del Río, J.; Gasulla, M. Effect of the Sampling Parameters in FOCV-MPPT Circuits for Fast-Varying EH Sources. *IEEE Trans. Power Electron.* **2023**, *38*, 2695–2708. [CrossRef]
19. Sher, H.A.; Murtaza, A.F.; Noman, A.; Addoweesh, K.E.; Al-Haddad, K.; Chiaberge, M. A New Sensorless Hybrid MPPT Algorithm Based on Fractional Short-Circuit Current Measurement and P&O MPPT. *IEEE Trans. Sustain. Energy* **2015**, *6*, 1426–1434.
20. Morales, R.H.; Rohten, J.A.; Garbarino, M.N.; Muñoz, J.A.; Silva, J.J.; Pulido, E.S.; Espinoza, J.R.; Andreu, M.L. A Novel Global Maximum Power Point Tracking Method Based on Measurement Cells. *IEEE Access* **2022**, *10*, 2169–3536.
21. Melo, F.C.; Garcia, L.S.; de Freitas, L.C.; Coelho, E.A.A.; Farias, V.J.; de Freitas, L.C.G. Proposal of a Photovoltaic AC-Module With a Single-Stage Transformerless Grid-Connected Boost Microinverter. *IEEE Trans. Ind. Electron.* **2018**, *65*, 2289–2301.

22. Noge, Y.; Yamaguchi, M.; Miyashita, M.; Deng, M. Experimental verification of buck-boost converter based micro inverter for minimization of magnetic components. In Proceedings of the International Conference on Electrical Machines and Systems (ICEMS), Sydney, Australia, 11–14 August 2017; pp. 1–5.
23. Hasan, R.; Hassan, W.; Xiao, W. PV Microinverter Solution for High Voltage Gain and Soft Switching. *IEEE J. Emerg. Sel. Top. Ind. Electron.* **2022**, *3*, 352–361. [CrossRef]
24. Zhang, F.; Xie, Y.; Hu, Y.; Chen, G.; Wang, X. A Hybrid Boost–Flyback/Flyback Microinverter for Photovoltaic Applications. *IEEE Trans. Ind. Electron.* **2022**, *67*, 308–318. [CrossRef]
25. Rajeev, M.; Agarwal, V. Analysis and Control of a Novel Transformer-Less Microinverter for PV-Grid Interface. *IEEE J. Photovoltaics* **2018**, *8*, 1110–1118. [CrossRef]
26. Hernandez-Vidal, R.; Surirey, Q.; Renaudineau, H.; Kouro, S.; Cabon, B. Push-pull based pseudo DC-link PV microinverter. In Proceedings of the Annual Conference of the IEEE Industrial Electronics Society, Beijing, China, 29 October–1 November 2017; pp. 7843-7848.
27. Tseng, K.-C.; Li, I.-C.; Cheng, C.-A. Integrated Buck and Modified Push-Pull DC-DC Converter With High Step-Down Ratio. *IEEE Trans. Ind. Electron.* **2020**, *67*, 235–243. [CrossRef]
28. Palma, L. Single Stage Quasi-Z-Source Push-Pull based Microinverter for On-Grid PV Applications. In Proceedings of the International Conference on Clean Electrical Power (ICCEP), Otranto, Italy, 2–4 July 2019; pp. 433-437.
29. Muñoz, J.; Díaz, M.; Rivera, M.; Dekka, A. Push-Pull Microinverter based on a Sub-modular Structure. In Proceedings of the International Symposium on Power Electronics, Electrical Drives, Automation and Motion (SPEEDAM), Sorrento, Italy, 22–24 June 2022; pp. 883–888.
30. Wu, Q.; Wang, Q.; Xu, J.; Li, H.; Xiao, L. A High-Efficiency Step-Up Current-Fed Push–Pull Quasi-Resonant Converter with Fewer Components for Fuel Cell Application. *IEEE Trans. Ind. Electron.* **2017**, *64*, 6639–6648. [CrossRef]
31. Mathew, D.; Naidu, R.C. Investigation of single-stage transformerless buck-boost microinverters. *IET Power Electron.* **2020**, *8*, 1487–1499. [CrossRef]
32. Knabben, G.C.; Schmitz, L.; Coelho, R.F.; Cruz Martins, D.; Custódio, O.J.; de Medeiros, R.Z.; Bettiol, A.L. Transformerless micro-inverter for grid-connected photovoltaic systems. In Proceedings of the International Universities Power Engineering Conference (UPEC), Heraklion, Greece, 28–31 August 2017; pp. 1–6.
33. Paul, A.R.; Bhattacharya, A.; Chatterjee, K. A Novel SEPIC-Ćuk Based High Gain Solar Micro-Inverter for Integration to Grid. In Proceedings of the National Power Electronics Conference (NPEC), Tiruchirappalli, India, 13–15 December 2019; pp. 1–5.
34. Bhattacharya, A.; Paul, A.R.; Chatterjee, K. A Single Phase Single Stage SEPIC-ĆUK Based Non-Isolated High Gain and Efficient Micro-Inverter. In Proceedings of the IEEE 46th Photovoltaic Specialists Conference (PVSC), Chicago, IL, USA, 16–21 June 2019; pp. 0708–0715.
35. Dong, D.; Agamy, S.; Harfman-Todorovic, M.; Liu, X.; Garces, L.; Zhou, R.; Cioffi, P. A PV Residential Microinverter With Grid-Support Function: Design, Implementation, and Field Testing. *IEEE Trans. Ind. Appl.* **2018**, *54*, 469–481.[CrossRef]
36. Wu, D.; Wu, Y.; Kan, J.; Tang, Y.; Chen, J.; Jiang, L. Full-Bridge Current-Fed PV Microinverter With DLFCR Reduction Ability. *IEEE Trans. Power Electron.* **2020**, *35*, 9541–9552. [CrossRef]
37. Tayebi, S.M.; Batarseh, I. Mitigation of Current Distortion in a Three-Phase Microinverter With Phase Skipping Using a Synchronous Sampling DC-Link Voltage Control. *IEEE Trans. Ind. Electron.* **2018**, *65*, 3910–3920. [CrossRef]